Journal of Alloys and Compounds 682 (2016) 42–51

Contents lists available at ScienceDirect

Journal of Alloys and Compounds

journal homepage: http://www.elsevier.com/locate/jalcom

Structure and properties of sputter-deposited Al-Sn-N thin films

Erik Lewin [a, b, *], Jörg Patscheider [a]

[a] Laboratory for Nanoscale Materials Science, Empa, Überlandstrasse 129, CH-8600, Dübendorf, Switzerland
[b] Inorganic Research Programme, Department of Chemistry – Ångström Laboratory, Uppsala University, Box 538, SE-751 21, Uppsala, Sweden

ARTICLE INFO

Article history:
Received 21 December 2015
Received in revised form
25 April 2016
Accepted 26 April 2016
Available online 28 April 2016

Keywords:
Nanocomposite
Coating
Sputtering
Hardness
Optical properties
Al-Sn-N

ABSTRACT

Coatings consisting of Al, Sn and N have been deposited using co-sputtering from Al and Sn targets in a reactive atmosphere containing N_2. AlN was used as starting point, and the Sn content was gradually increased through higher cathode power on the Sn target, resulting in coatings with Sn-contents between 0 and 24 at.%. The coatings were analysed using X-ray diffraction (XRD), X-ray photoelectron spectroscopy (XPS) and scanning electron microscopy (SEM) and also characterised using UV–vis spectroscopy and nanoindentation.

All coatings show a nitrogen content of about 50 at.% and are thus fully nitrided, which is confirmed by bonding analysis with XPS. A combination of results from XRD and XPS leads to the conclusion that the coatings consist of a single phase solid solution based on wurzite $(Al_{1-x}Sn_x)N_y$ with x varying between 0 and 0.5, and y close to unity. The attained material is metastable with respect to decomposition into AlN, Sn and N_2, as shown by sputter damages occurring during Ar^+ ion etching. The top surface and cross sections, as observed in SEM, were found to become smoother and the columnar structure less pronounced, changing to grainy and finally glass like morphology, as the Sn content is increased.

The material is hard at room temperature, with nanoindentation values of 17–24 GPa. Coatings on silica substrates are transparent and yellow to red-brown in colour. This is quantified as a shifting absorption edge, which moves from 211 to 510 nm, corresponding to an optical band gap of 5.9 and 2.4, respectively, as the Sn-content is increased. The index of refraction varies between 2.0 and 2.6. The deposited materials are thus hard, and have a tuneable absorption edge, which could be applicable in optical applications as a multifunctional optical filter with scratch resistant properties.

1. Introduction

A successful way of forming new and modified coating materials is to add a third element to a binary hard coating material, and thereby form a ternary material. What kind of microstructure which is attained, is commonly a function of the concentration of the third element: unless strong repulsive forces exist between the third element and the binary material solid solutions are usually formed at low concentrations. At higher concentrations, above the limit of solid solution, thus provoking phase segregation, nanocomposites may form, while in some cases amorphous phases are formed, usually at high concentrations under conditions of low surface mobility. This kind of alloying has been extensively studied for TiN- and TiC based material by using most commonly Al, Si [1–10], but also studies with Ge and Sn exist [11,12]. Less extensively studied are ternary materials based on the optically transparent compound AlN. Studies have e.g. been conducted adding B for altering piezoelectrical properties tuning of band gap or for LED devices [13–15], with a focus on optical and mechanical properties the addition of Si or Ge [16–25] has also been investigated. The addition of B, Si or Ge to AlN during thin film growth all lead to the formation of a (metastable) solid solution phase at low alloying concentrations; the formation of a secondary phase, and thus a nanocomposite microstructure is found at higher alloying concentrations. Both these changes, compared to the binary AlN, will lead to changes in the coating properties and performance, which can be utilised for materials design.

The present study stands in line with previous studies on Al-A-N material (A = Si or Ge) using unbalanced magnetron sputtering [17,18,20–23,26], and has the aim to investigate the Al-Sn-N system, with a focus on mechanical and optical properties. The purpose of the present study is to expand the materials design

* Corresponding author. Inorganic Research Programme, Department of Chemistry – Ångström Laboratory, Uppsala University, Box 538, SE-751 21, Uppsala, Sweden.
E-mail address: erik.lewin@kemi.uu.se (E. Lewin).

http://dx.doi.org/10.1016/j.jallcom.2016.04.278

concepts from the previously studied Al-A-N materials and elucidate the chemical and microstructural relations between these ternary thin film materials. Previous studies [17,18,20–23,26] have in general found the Al-A-N (A = Si or Ge) system to exhibit similar structures and properties, with sputter deposited coatings consisting of an AlN-based solid solution phase $(Al_{1-x}A_x)N_y$ and at higher concentrations of the third element A also a second, amorphous, AN_z phase thus forming nanocomposites. A transition from a single phase regime to a bi-phased material, which was interpreted as the solid solution limit of Si in AlN, was found to be about 6 atomic percent (at.%), and for Ge about 12 at.% under fully comparable conditions. The coatings were found to be hard in the range of 16–30 GPa with a shallow maximum corresponding to a microstructure where the A-saturated nanocrystalline Al-A-N phase was separated by small amounts of AN_z matrix. This is consistent with a so-called nanocomposite hardening also observed for systems such as nc-TiC_x/a-C [27–29] and nc-TiN/Si_3N_4, [3,30] although in less pronounced form. The coatings are generally optically transparent at near infrared (NIR) and visual (vis) wavelengths, with the Al-Si-N materials having an absorption edge about 220–270 nm, corresponding to an optical band gaps (E_{04}) of 5.6 to 4.6 eV. The Al-Ge-N coatings had a tuneable absorption edge between 220 and 340 nm, corresponding to a range of the optical band gap (E_{04}) of 5.6 to 3.6 eV. Also the index of refraction could be controlled in these materials, with a range between 2.0 and 2.5, although not independently from the band gap.

No ternary Al-Sn-N phase diagrams or phases are available in the existing literature, neither is any work at all retrievable that is dedicated to the ternary Al-Sn-N system. A look at the related phase diagrams in literature [31–35] gives no other expected compound phases than AlN. No phase diagram has been composed for the N-Sn system, however a metastable tin nitride phases is reported in literature, see below.

The two nitrides expected to be found in sputtered coatings in the Al-Sn-N material are AlN and SnN_x. Aluminium nitride (AlN) is a covalently bonded nitride, which crystallizes in the hexagonal wurtzite structure. AlN is a well-known wide band gap III–V semiconductor with high thermal conductivity and good thermal stability as well as chemical inertness and mechanical strength. Pure AlN thin films have a hardness of about 20–22 GPa, a refractive index of 2.1–2.2, and a band gap of 5.9–6.0 eV and are thus fully transparent in the NIR, visible, UV-A and UV-B spectral regions. AlN sublimates at temperatures above 2200 °C, is inert to strong acids and bases, but dissolves slowly in boiling water [17,36–40]. Coatings of AlN can be produced by sputter deposition, and there are extensive studies available on growth of different orientations and microstructures [41–47].

Two Sn-N phases are reported in the literature, one hexagonal [48] and one cubic [49]. However, a closer inspection of the diffraction patterns reveals that the pattern assigned to the hexagonal phase also can be indexed by the cubic phase. It is noteworthy that the works referring to the hexagonal structure pertain to thin film materials, but the works referring to the cubic structure mainly are on bulk materials. The cubic structure is a spinel structure with Sn occupying both octahedral and tetrahedral metal positions, giving the formula Sn_3N_4 [49]. This structure is isostructural with γ-Si_3N_4 and γ-Ge_3N_4, and *ab-initio* materials simulations have shown this structure to be metastable with respect to metallic Sn and N_2, although more stable than the α- or β-phases (that exist for Si_3N_4 and Ge_3N_4) [50]. There are a substantial number of reports available on amorphous Sn-N, where the elemental composition of the reported materials varies in a wide range. According to these previous findings, we will use the general notation SnN_x throughout this manuscript.

The above mentioned metastability is experimentally confirmed by commonly observed damage upon sputter-etching of samples before XPS (X-ray photo electron spectroscopy) or AES (Auger electron spectroscopy) analysis [48,51–53], as well as by the fact that it decomposes into the elements upon heating in inert atmosphere (reported decomposition temperatures between 420 °C and 615 °C [54–57]), and may oxidize if left in the lab, which was observed already in the earliest studies [58,59]. However, later studies have also reported that γ-Sn_3N_4 is stable in vacuum up to 300 °C [49].

This variation in reported material properties is quite typical for the literature on SnN_x, as it seems to be difficult to produce phase pure and fully nitrided samples. Owing to its low stability there are also problems in determining the stoichiometry of SnN_x samples, e.g. due to spontaneous oxidation, decomposition and sputter damage when sputter-cleaned prior to XPS. Thus it is from literature difficult to ascertain the exact physical properties of SnN_x. Generally SnN_x is reported to be a semiconductor with resistances in the range of 2–150 mΩcm [51–53,55,56,60], where dependence on both composition and structure (amorphous or crystalline) have been observed [51]. The band gap of SnN_x is reported in the range of 1.5–4.9 eV, although most commonly below 2 eV [50–53,56,57,61,62]. For both these material constants measured values can be heavily influenced by both metallic (due to low nitiridation during synthesis) and oxide (due to the low stability and subsequent oxidation in air) contributions to the sample, which is probably the reason for the observed spread in values. The colour of the material (as powder or as a coating on transparent substrates) is reported to be between yellow, red and light brown [50,51,53,55,63], which corresponds to the observed band gaps. Connected to this is also the reported electrochromic behaviour of tin nitride, which later was found to be an irreversible process involving reduction of the tin nitride to tin and subsequent oxidation to tin oxide, when polarity was reversed [57]. Also the reported values for the index of refraction also vary drastically, between 1.5 and 3.3 [53,61]. Only one report exists on the mechanical properties of tin nitride, where crystalline and amorphous coatings were found to be harder than SiO_2 and SnO_2 [51].

Coatings of tin nitride have been deposited through various forms of sputtering (diode or magnetron, using DC or RF discharges) [48,51,52,56,57,59,62–65] and several forms of CVD [53,55,61,66]. In general, both crystalline [48,51–53,56,57,66] and amorphous [51,53,57,61–63,65] material can be attained, depending on deposition process and conditions.

Considering the coatings prepared in previous work on the Al-Si-N and Al-Ge-N systems, their trends as well as the available literature on SnN_x, it was thus expected that co-sputtering of Al and Sn in a reactive nitrogen atmosphere will give an AlN-based solid solution phase at low Sn contents; and at higher Sn contents a formation of a second Sn-based phase – probably an amorphous SnN_x. Due to the low thermodynamic stability there is a high probability that the attained coatings will be N-deficient. It is also expected that optical properties as absorption, band gap and refractive index will be influenced, and probably different properties attained compared to both AlN and Al-Si/Ge-N materials.

2. Experimental details

Coatings were synthesised by reactive magnetron sputtering in an AJA 1500C sputter system, described in detail elsewhere [17]. The base pressure during the present depositions was $1.0 \cdot 10^{-8}$ mbar or below. Sputter deposition was performed from 2″ elemental targets of Al and Sn, using a confocal sputter-up geometry with a distance of 12 cm between targets and substrates. Depositions were carried out at a constant pressure of 6.0 μbar with gas flows of 20

sccm N_2 gas, i.e. in a pure N_2 atmosphere. Prior to the deposition the substrate holder was typically heated to 200 °C by heating lamps on the backside, and the temperature was maintained during the entire process. During deposition the substrate holder was RF-biased to −60 V. Additional experiments were also conducted at slightly different conditions, employing either no bias (floating potential), lower substrate temperatures (unheated), or running the process in a mixed N_2/Ar atmosphere with the mass flow ratio 1:2. The composition was varied by changing the power on the Sn target (0–45 W), whilst applying a constant power to the Al target (250 W). Deposition time was varied to attain coatings with a thickness of about 1.5 μm.

Depositions were carried out simultaneously on substrates of Si(100), a-SiO_2 and compliant polyimide substrates (Kapton, a temperature-resistant polymer, used for XRD (X-ray diffraction) analysis, see below). Prior to introduction into vacuum, the substrates were ultrasonically cleaned in acetone and ethanol, and then dried in an inert gas flow. Just prior to deposition, in-situ plasma cleaning was performed using an Ar plasma at a RF-bias of −75 V. This plasma cleaning is expected to remove organic residues, but not the native oxide on the Si substrate, nor does it damage the Kapton substrates.

The crystalline phase content of the samples was evaluated with XRD using two different diffractometers, both employing Cu Kα radiation. Samples on SiO_2 were analysed using a Bruker D5000 diffractometer equipped with an Euler cradle and either Bragg-Brentano optics for θ/2θ scans, or parallel beam optics with an acceptance angle of 0.40° for grazing incidence (GI) scans. Measurements on coatings on the conforming polyimide substrate were conducted using a PANalytical X'Pert Pro diffractometer equipped with a Goebel mirror and a parallel plate collimator with an acceptance angle of 0.27°.

XPS was performed using a Physical Electronics Quantum 2000 spectrometer, which employs monochromatic Al Kα radiation, a 45° photoelectron take-off angle, and has an optimal resolution of 0.50 eV. Bulk compositions were determined from XPS using sputter depth profiles; sensitivity factors were derived from reference measurements of three samples using a combination of elastic recoil detection analysis (ERDA) and Rutherford backscattering (RBS). For the range 4–12 at.% Sn the differences in the composition values determined by XPS, RBS and ERDA were below ± 0.7 at.%, indicating the robustness of the calibration. Chemical bonding in the samples was determined using high resolution (compared to the depth profiles) XPS scans after sputter etching to a depth of approximately 30 nm, thus giving data from the bulk of the coating. If not otherwise stated, low energy Ar^+ ions (200 eV) were used for sputter etching in order to minimize sputter damage. Additional experiments were performed using higher Ar^+ energies, and using an in-situ transfer chamber (which eliminates the necessity of sputter cleaning) to evaluate the extent of sputter damage. All XPS characterization was carried out on coatings on Si substrates and under constant neutralization using an electron flood gun and very low energy Ar^+ ions, as described by Larson et al. [67] Ion beam analysis (RBS [68] and ERDA [69]) to determine the sensitivity factors for XPS was performed at the Laboratory for Ion Beam Physics of ETH, Zürich. RBS measurements were performed using a 2 MeV ^{4}He beam and a silicon surface barrier detector under 168°. The collected RBS data were simulated using the RUMP software [70]. For the ERDA analysis a 13 MeV ^{127}I beam was used under an 18° incidence angle. The scattered recoils were identified by the combination of a time-of-flight spectrometer and a gas ionization chamber. The data was analysed by means of the DataFurnace code [71].

The coating morphology was observed by scanning electron microscopy (SEM) on fractured cross sections of coatings on Si substrates. SEM was performed using a FEI NanoSEM 230, operated at 15 kV in high-vacuum mode. Prior to the measurements samples were coated with a thin carbon layer by evaporation to improve conduction. No artefacts from the carbon coating could be observed on the fractured (and smooth) substrate surfaces at the used magnifications, thus ensuring that observed structures in the coatings are features of the studied material.

Nanoindentation was performed to determine Hardness and Young's modulus. Measurements were performed on a Hysitron Ubi using a Berkovich diamond tip. Indents were performed to a maximum load of 3.5 mN, which yielded indentation depths of 75–87 nm (i.e. 4–8% of the coating thicknesses), thus minimizing the influence of the substrate. At least 20 indents per sample were performed, whereof at least 15 were used for data evaluation according to the method of Oliver and Pharr [72] using software supplied by the instrument manufacturer. Reference measurements on fused silica, using the same parameters as for the coatings, yielded a hardness of 9.1 ± 0.1 GPa and Young's modulus of 68.0 ± 0.4 GPa, thus in reasonable agreement with literature. To obtain a measure of macroscopic stresses on coatings deposited on Si, profilometry was performed and the total residual stress calculated using Stoney's equation [73–75]. For the calculations the literature values of the biaxial modulus for Si(100) were used. Measurements were performed using a Tencor P10 needle profilometer, with two approximately orthogonal 5 mm longs scans, from which an average stress was calculated.

Optical measurements to determine the transmission, absorption coefficient and refractive index were performed using a Shimadzu UV-3600 UV–Vis–NIR spectrometer. Data were evaluated using the envelope method, which allows the determination of the aforementioned parameters from a single transmission spectrum with interference fringes [76,77]. The presented values for optical constants as function of wavelength have been attained through interpolation between the values at the fringe positions. Electrical resistivity was tested with a simple 4-point-probe set-up.

3. Results

3.1. Initial experiments and process selection

Hysteresis experiment, conducted with constant pumping speed, target power and total gas flow, show distinct poisoning of the Al target (slope change in current), but none for the Sn target. No change in the slope of the total pressure curve was observed. This indicates that no surface compound formed on the Sn target, and thus that deposited material is expected to be N-deficient, even if a pure N_2 atmosphere is used. Material attained using a pure N_2 atmosphere was although transparent and yellow to reddish brown in transmission, depending on concentration, in contrast to coatings deposited in mixed Ar/N_2 atmosphere which were opaque, indicating presence of metallic Sn^0.

Coatings deposited in a pure N_2 atmosphere were found to have considerably larger oxygen content than those from mixed Ar/N_2 atmosphere, which is correlated to a considerably more porous microstructure, as observed in SEM (not shown). To counteract this, an RF substrate bias of −60V was employed, which led to denser coatings and less oxygen in coatings as measured in ex-situ XPS. The dense coatings deposited using the −60V RF bias and pure N_2 atmosphere were less columnar than the incompletely nitrided coatings deposited from N_2/Ar gas mixtures prepared without bias.

It is also worth noting that the coating composition changed markedly as the sputtering gas was changed: the Sn content was found to be smaller for coatings deposited using only N_2, compared to an Ar/N_2 mixture. This has most likely its explanation in the lower mass of N^+ compared to Ar^+ giving les efficient sputtering of

the heavier Sn atoms (compared to Al atoms).

Attempts to synthesise a SnN_x reference sample were unsuccessful. Coatings deposited using only N_2 as sputtering gas and −60V RF bias were opaque, and samples deposited without bias (floating) are less opaque (difficult to determine due to different thicknesses), but oxidised when stored in the lab before analysis could be performed, probably due to an underdense microstructure.

Thus, the main sample series studied in the present work were deposited in a pure N_2 atmosphere and using an RF bias of −60 V. No binary SnN_x reference sample is included, and the binary AlN reference was deposited with a floating bias, as it otherwise had too large residual compressive stresses, leading to severe delamination. As expected, the deposition rate was found to vary with Sn content, with 33 Å/min for the binary Al-N sample and 87 Å/min for the sample with highest Sn content. Samples included here had coating thicknesses between 1.2 and 2.0 μm.

3.2. Composition, phase identity and microstructure

3.2.1. X-ray photo electron spectroscopy

Coatings were deposited in several series with varying power to the Sn target, and subsequently varying composition, see Fig. 1. They have Sn contents between 0 and 24 at.%, and subsequently Al contents between 43 and 26 at.%. The nitrogen content was roughly constant, although slightly decreasing with Sn-content from 54 to 50 at.%. The accurate compositional determination is hampered by the susceptibility of these coatings to sputter damages, especially at elevated Sn contents. However, considering the used calibration against RBS/ERDA measurements for samples with Sn-contents of 4–12 at.%, which gave a precision of ±0.7 at.%, the errors are at most a few at.%. The oxygen content is generally low, with all ternary coatings showing oxygen contents below 0.8 at.%. The binary AlN reference (which was deposited without substrate bias) had a slightly higher oxygen content of 3 at.% (which is mirrored by a slight decrease in nitrogen concentration), probably due to an underdense structure, facilitating ex-situ oxidation (see e.g. Pélisson-Schecker et al. [26]). The samples in Fig. 1 were deposited in five series up to 10 months apart; the small spread of data points illustrates that the experimental reproducibility with regards to composition is high.

Bonding characterization was carried out by high resolution XPS in the bulk of the coatings; the spectra are shown in Fig. 2 which shows a total of 15 spectra for each region. As can be seen, all the ternary samples (solid lines) exhibit almost identical spectra, thus indicating identical chemical surrounding for respective elements, irrespective of the Sn concentration. The only spectra that differ slightly are those from the binary AlN reference (dashed line), which (naturally) doesn't have any Sn 3d peaks, and has a slightly smaller line width for the N 1s peak (Fig. 2c) (full width at half maximum, fwhm, of 1.34 eV compared to 1.60 eV in average). This indicates that there are more than one (but mainly overlapping) chemical environments for N in the ternary Al-Sn-N samples.

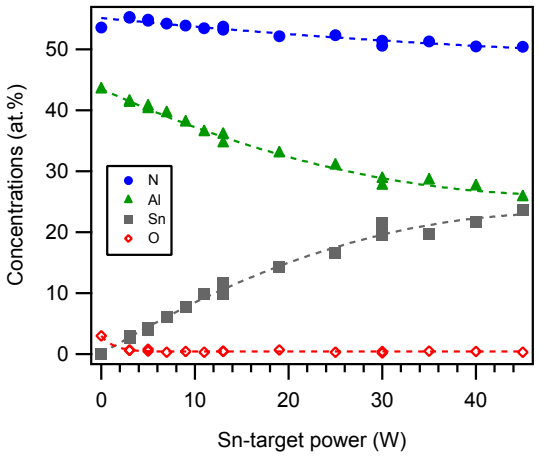

Fig. 1. Composition of the sputtered Al–Sn–N coatings, as determined from XPS sputter depth profiles. Lines are only intended as guides for the eye.

The Al 2p peak (Fig. 2a) has been used for charge referencing, and its binding energy has been set to the literature value for AlN of 73.6 eV [78,79]. The usefulness of this simple approach is evident by the good alignment of peaks observed in the other spectral regions (Figs. 2b and c, respectively). The observed binding energy for Sn $3d_{5/2}$ (486.22 ± 0.07 eV) and N 1s (396.74 ± 0.04 eV) are both good matches to literature values of SnN_x (Sn $3d_{5/2}$ at 486.0–486.8 eV, and N 1s at 396.3–397.3 eV) [51–53,55,57,65] and AlN (N1s at 396.5–397.0 eV) [78,79]. Also the observed binding energy differences between the nitrogen and respective metal peaks, $\Delta(Sn3d_{5/2} - N1s) = 89.46 \pm 0.04$ eV and $\Delta(N1s - Al2p) = 323.14 \pm 0.04$ eV, which are independent of charge referencing and E_b-scale calibrations, are also in good agreement with literature values (88.9–89.6 eV and 322.8–323.8 eV, respectively) [51,52,55,65,66,79]. It can thus be concluded that both Al and Sn atoms have a chemical surrounding matching the respective nitride, i.e. both metals are bonded to nitrogen. The broadening of the N 1s peak increases markedly (by a factor of 1.2) for the ternary samples (solid lines) compared to the binary AlN sample (dashed line), see Fig. 2c. In the case of a random substitution of Al with Sn in the material, five different quasi-tetrahedral surroundings are possible for N ($NAl_{4-x}Sn_x$, with x is a discrete number between 0 and 4). Thus, several different chemical states can exist, and the observed broadening for the ternary samples is consistent with a solid solution nitride.

In the Sn 3d spectra (Fig. 2b) there is a small asymmetry of the peaks towards lower binding energy, indicating the presence of a small metallic (Sn-Sn) contribution. This is an artefact due to sputter damage, and is more pronounced, if higher Ar^+ energies (than the here used 200 eV) are used for sputter etching. Measurements on pristine samples transferred from the deposition chamber *in-vacuo* (thereby eliminating surface oxidation and need for sputter-cleaning before analysis) confirm that undamaged samples do not have this asymmetry. These measurements are not shown in the present paper, but will be published in a separate paper. Furthermore, these measurements show that valence band region is heavily influenced by sputter-damage, also using such low ion energies as 200 eV. For this reason the valence band region is not shown for the present samples.

3.2.2. X-ray diffraction

X-ray diffraction data attained from samples on silica substrates are shown in Fig. 3. The bottom diffractograms in both graphs show the binary AlN reference sample. They agree very well with the literature data (vertical markers at bottom of graphs) for hexagonal wurzite AlN [80]. As the Sn content is increased (upward in Fig. 3) three main observations can be made: Firstly, from both the grazing incidence (GI) (a) and the symmetrical θ/2θ (b) scans it is evident that the peaks in the wurzite pattern are shifted to lower diffraction angles, indicating larger lattice spacings. Secondly, there is a distinct peak broadening, indicating smaller crystallites at higher Sn concentrations. Thirdly, as evident from the θ/2θ scans, there are changes in preferred orientation. All of these observations are discussed in detail below.

To eliminate any effect of coating stresses on the measurement of lattice distances, coatings were also deposited on conforming

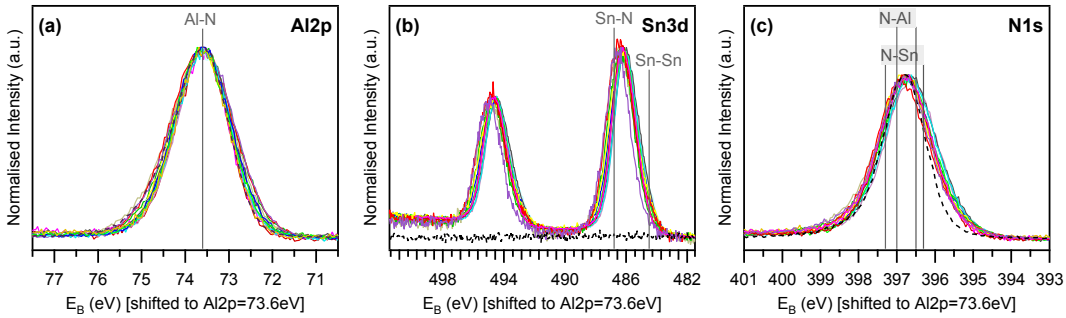

Fig. 2. High resolution XPS spectra from 15 samples with Sn contents between 0 and 24 at.%. The dotted line shows the binary AlN reference, other samples are ternary Al–Sn–N samples. Spectra have been normalised. Charge referencing has been performed using the Al 2p line and setting it to 73.6 eV, which is the literature position for AlN [78,79]. Vertical lines mark literature position/ranges for respective types of bonds [51–53,55,57,65,78,79].

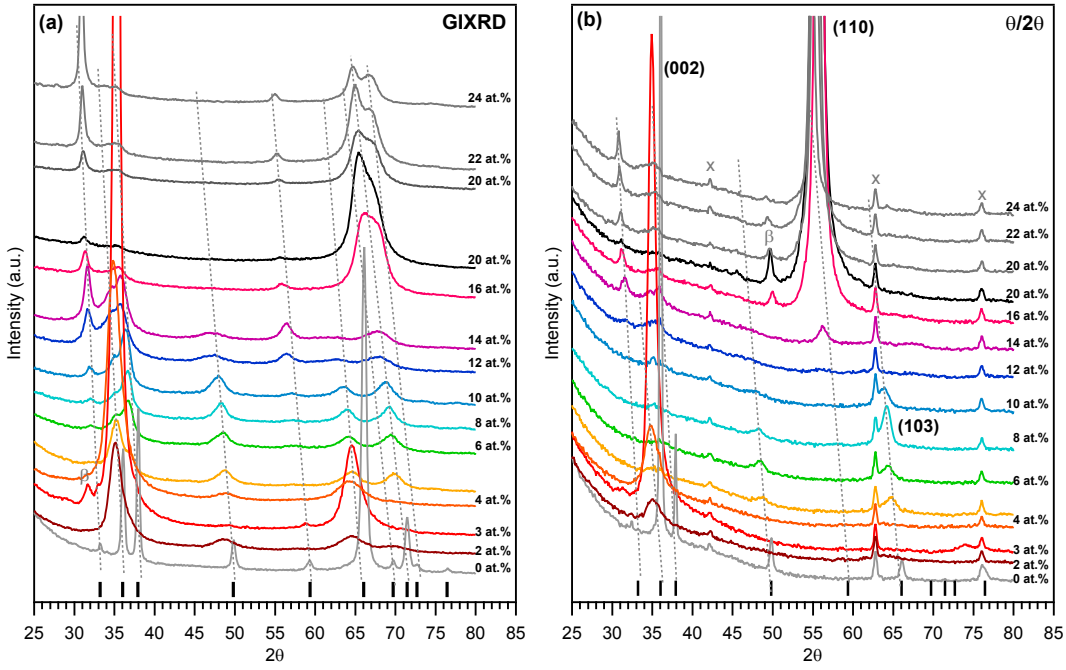

Fig. 3. Diffractograms from Al–Sn–N samples deposited on a-SiO_2 substrates: a) grazing incidence, and b) θ/2θ. Vertical markers at the bottom of each diffractogram show literature reference positions for hexagonal wurzite AlN phase [80]. Slanted lines mark the evolution as a function of Sn content. In (b) Miller indices mark the three main peaks corresponding to observed preferential orientation, "x" mark peaks from the substrate holder, and "β" peaks due to Cu Kβ-radiation. Sn content of the samples is increasing upwards in the graphs. The diffractograms have been offset in y, but not scaled, thus their intensities are comparable.

polyimide substrates and analysed with XRD. The observed diffraction patterns were (with exception of some minor substrate contributions) practically identical to those present in Fig. 3. Only small changes in peak positions were observed, due to the elimination of residual stresses. The relative expansion compared to literature values of AlN [80] calculated from both θ/2θ and GI scans of these samples are presented as a function of Sn content is in Fig. 4. As can be seen, the lattice expansion follows the same, roughly linear, trend for all observed diffraction peaks, in both measuring geometries. This indicates that the expansion is isotropic, with regards to both crystal and spatial directions. This also shows that the wurzite structure of the AlN phase is retained, but linearly expanded up to about 7%, which must be considered extreme. Such a lattice expansion is consistent with a solid solution of Sn in the AlN-phase, i.e. $(Al_{1-x}Sn_x)N$ with x in this case up to at least 0.5.

As is evident from Fig. 3b there are changes in the preferred orientation of the wurzite phase, as the Sn content increases. This has been quantified by calculation of the Harris texture coefficient [81], where a value above 1 indicates that an orientation is more common than in a randomly oriented powder. The texture coefficients for three different diffraction peaks are shown as a function of Sn content in Fig. 5. As can be seen from both the texture coefficients and the diffractograms, the basal plane (002) texture common for AlN is retained at very low Sn contents (up to 3 at.%), and at high Sn contents (>14 at.%) a (110) texture is totally dominating. The samples in-between have a (103)-texture, but also with a clear polycrystalline contribution (all peaks visible in GI-scans). From the intensity in the θ/2θ-diffractograms (and also the value of the texture coefficient) it is although clear that this texture is not as extreme as the others.

The grain size reduction, estimated from peak broadening (full width at half maximum) and Scherrer's equation [82] using $k = 0.9$ and the data from samples on silica substrates, is given in Fig. 6. As can be seen, grain size is reduced as soon as the third element (i.e. Sn) is introduced and all ternary samples exhibit similar grain sizes

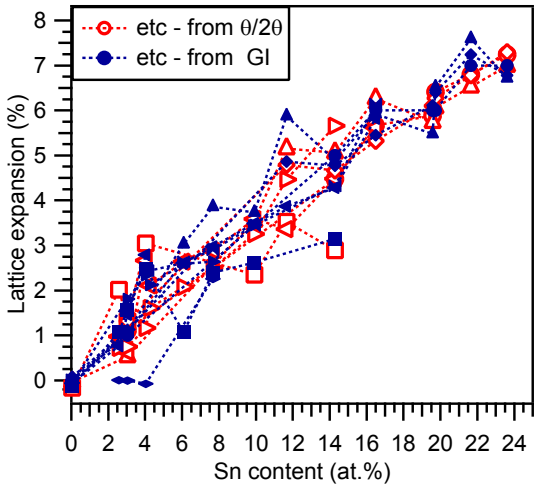

Fig. 4. Lattice expansion for the wurzite AlN-based phase, as observed in coatings deposited on conforming polyimide substrates. Data from both GI- and θ/2θ scans are shown; data from 8 peaks from GI, and 6 peaks from θ/2θ.

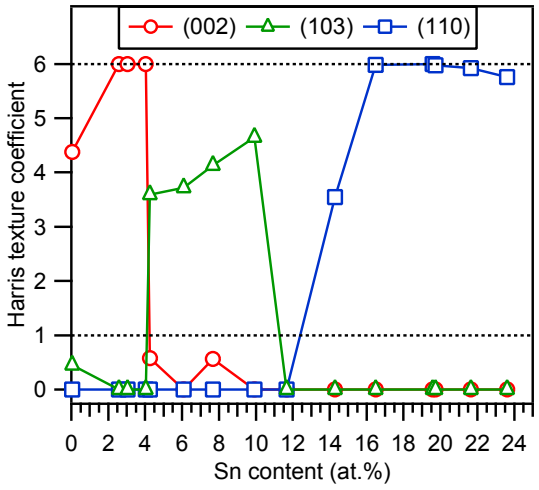

Fig. 5. Harris texture coefficient for the (002), (103) and (110) diffraction peaks, calculated using the six peaks observed in θ/2θ scans. Dashed lines indicate value for random orientation (1) and maximum texture (6).

with a combined average and uncertainty of 6 ± 1 nm. Generally similar grain sizes are observed from GI- (solid circles) and θ/2θ (open triangles) scans, thus indicating roughly isotropic grains. The exception is the AlN reference and the most textured samples with Sn contents of 16–20 at.%, which all exhibit slightly larger grain size in the growth direction.

Additionally there are two observations that can be made regarding the intensities in the diffractograms, which reflect the increased amount of heavy Sn atoms. In the GI-scans (Fig. 3a) it is evident that the background below $2\theta = 25°$, originating from the amorphous silica substrate, diminishes as the Sn content increases and with it the X-ray blocking power of the coating. Secondly, the maximum intensity attained for the heavily textured samples are very different for low and high Sn content, despite identical sample sizes and comparable thicknesses, the high Sn content samples exhibit much higher count rates (see Fig. 3b). This can be understood since Sn has a higher atomic number and therefore scatters X-rays much more efficiently than Al, and thus increases the diffracted intensity.

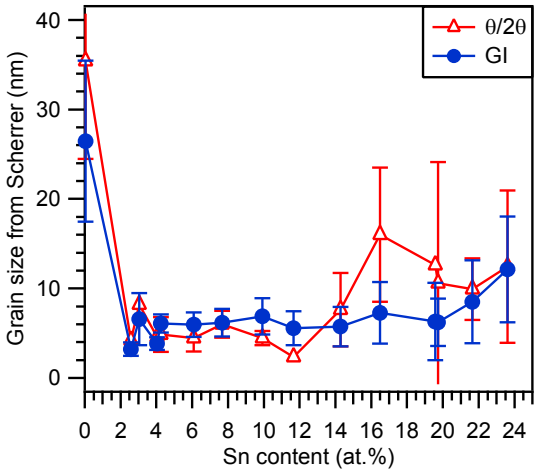

Fig. 6. Grain size (estimated through Scherrer's equation) as a function of Sn content. Data from both GI- (filled blue markers) and θ/2θ (open red markers) scans on samples deposited on silica. Values are averages from all observed diffraction peaks, and error bars indicate confidence intervals of 95%. (For interpretation of the references to colour in this figure legend, the reader is referred to the web version of this article.)

3.2.3. Electron microscopy

Scanning electron microscopy (SEM) images of representative Al-Sn-N samples of different Sn contents are shown in Fig. 7. As expected the binary AlN reference (far left) exhibits a clear columnar structure, and as Sn content increases (to the right) the columnar growth is disrupted and a more fine grained and finally almost glass-like morphology is attained. Also the top surfaces of the coatings follow the same trend.

3.3. Material properties

3.3.1. Mechanical properties

Hardness and Young's modulus of the coatings were measured by nanoindentation and are shown in Fig. 8. The coatings' hardness reaches values between 17 and 24 GPa, while the moduli lie between 161 and 212 GPa. In both cases a shallow maximum is observed about 3 at.% Sn, followed by a slowly decreasing trend towards higher Sn contents. The latter trend is interrupted by a sharp dip at 4 at.% Sn. This coincides with the distinct change in texture from (001) to (103) as observed by XRD, see Fig. 5.

Residual stresses in the coatings were analysed using the substrate bending method and Stoney's equation. All ternary coatings (deposited with a −60V substrate bias) were found to have compressive stresses between 1 and 2 GPa (aggregated average 1.5 ± 0.2 GPa); the binary AlN coating (which was deposited using a floating bias) had tensile stresses of about 500 MPa. Thus the observed hardness is not significantly increased by residual stresses.

3.3.2. Optical properties

Raw data from UV–vis–NIR transmission measurements are shown in Fig. 9. There are no other features than the thickness fringes and the absorption edge at lower wavelengths. It can clearly be seen that the absorption edge of the ternary coatings are significantly shifted to longer wavelengths, compared to the binary AlN reference. Furthermore, there is a clear trend pushing the absorption edge towards longer wavelengths, as the Sn content increases. This is quantified in the optical band gap E_{04} (i.e. the wavelength where the absorbance, α, exceeds 10^4 cm^{-1}), which is shown in Fig. 10a. As can be seen, the optical band gap drops from 5.9 eV (corresponding to an edge position of 211 nm) to 2.4 eV

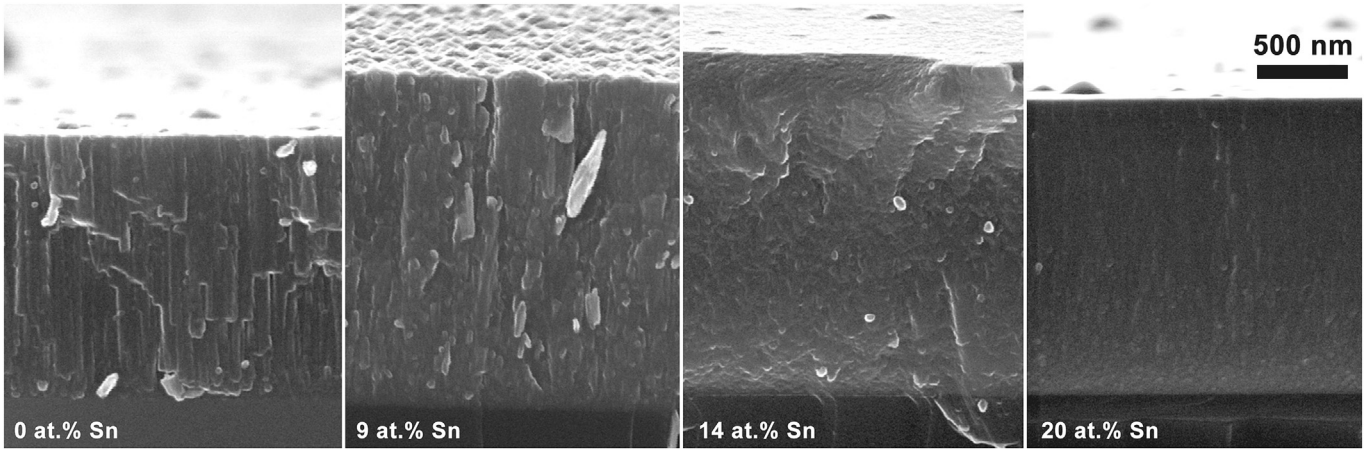

Fig. 7. SEM images of fractured cross sections of coatings with varying Sn content. Images acquired with a 3° tilt, thus giving a limited view of the coating top-surface. Images have been enhanced using brightness/contrast controls, as well as more advanced non-linear tools, but always on the entire image.

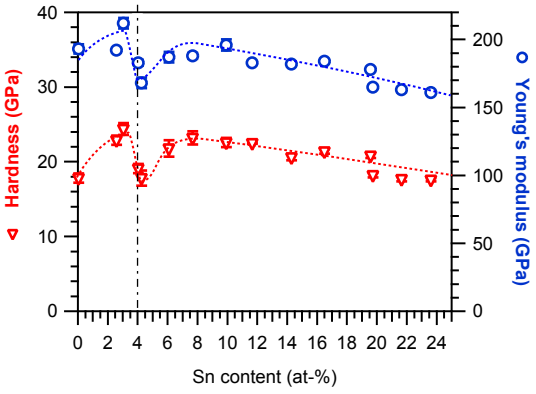

Fig. 8. Data from nanoindentation, showing hardness (left abscissa, triangles) and Young's modulus (right abscissa, circles) as a function of Sn content. Error bars show 90% confidence intervals. Lines are only intended as guides for the eye.

(corresponding to 512 nm), as the Sn content is increased from 0 to 24 at.%. This change in band gap is also accompanied by a change in refractive index (at 633 nm), which increases from about 2.0 to 2.6, see Fig. 10b. With the observed band gaps it is expected that the material is electrically insulating, which was confirmed by 4-point-probe measurements, were no conductivity was observed, i.e. resistivity is at least in the order of several tens of MΩcm.

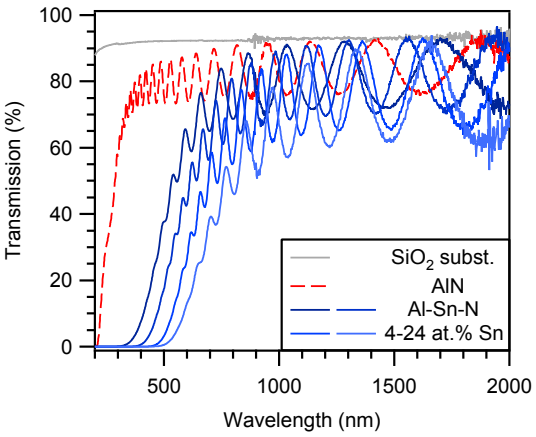

Fig. 9. UV–vis–NIR transmission spectra for binary and ternary coatings on fused silica substrates. The grey curve is a spectrum of a blank substrate. Shown samples have thicknesses between 1.2 and 1.8 μm.

4. Discussion

4.1. Microstructure

In the deposited samples only one crystalline phase is observed, a wurzite AlN-based phase. The presence of a secondary, amorphous, phase cannot be fully excluded without further analysis using e.g. transmission electron microscopy (TEM) or atom probe tomography (APT), which is beyond the scope of the present work. However, there are several indications that no secondary phase is formed. Firstly the continuously expanding lattice parameter, shown in Fig. 4, indicates that Sn is incorporated into the AlN lattice. If a secondary phase was formed, a break in the expansion is to be expected, which has been observed in the cases of alloying AlN with Si [17,18] and Ge [23]. Furthermore, in the case of Al-Ge-N [23] abrupt changes in the optical properties were observed, which are correlated to the formation of a secondary phase; here no such breaks can be observed, thus corroborating the interpretation as single phase samples. The observed texture change at ~13 at.% Sn (see Fig. 5), which is coupled with an elongation of the grains (c.f. crystallite sizes from GI- and θ/2θ scans in Fig. 6) could be indicative of a tissue phase formation. However, the lack of trend changes in lattice expansion and optical properties makes this unlikely. As stated above, further studies are needed to reach full clarity.

The formed phase is based on wurzite AlN, which is proven by the diffraction pattern, although with varying lattice spacings. The relative expansion follows the same linear trend for all peaks, both in GI- and θ/2θ-measurements, clearly indicating that the expansion is isotropic with respect to both crystal directions and to substrate directions, which is consistent with an isotropic solid solution phase. The solid solution is achieved by substitution on the metal lattice and shown by the XPS results, where Sn-N coordinations are observed as well as Al-N, as in binary AlN. Therefore the formed solid solution phase can be described as $Al_{1-x}Sn_xN_y$ with $x_{max}<0.5$. A comparison of the observed expansion (~7%) using a simple Vegard-like linear interpolation between the average bond lengths of Al-N (1.90 Å) and Sn-N (2.14 Å) from the structures reported in literature for wurtzite AlN [80] and γ-Sn_3N_4 [49] illustrates the single-phase solid solution nature of the investigated coatings: the expected average bond length from those literature data at x = 0.5 is 2.02 Å, or an expansion of 6.3% compared to AlN and thus quite similar to the linear trend reported in Fig. 4 with a

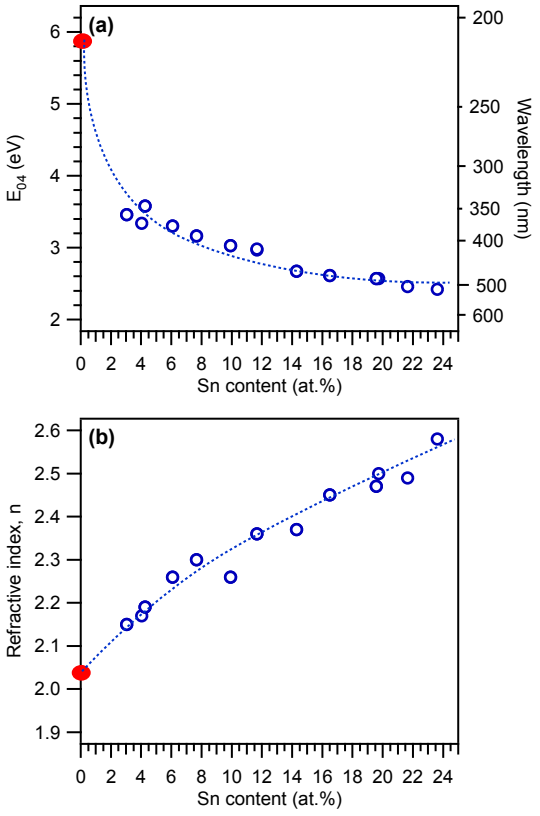

Fig. 10. Optical data as a function of Sn content of the samples, calculated from transmission spectra shown in Fig. 9 a) Optical band gap (E_{04}) and absorption edge position as defined by an absorbance of 10^4 cm^{-1}. b) Index of refraction at 633 nm. Solid (red) marker shows binary AlN coating, and open (blue) markers show ternary samples. Lines are only intended as guides for the eye. (For interpretation of the references to colour in this figure legend, the reader is referred to the web version of this article.)

value of about 7 at.% at x = 0.5, corresponding to a bond length of 2.03 Å.

Such as solid solution phase is expected to be metastable due to the weak bonds between tin and nitrogen. The calculated enthalpy of formation of γ-Sn_3N_4, the least unstable modification, amounts to +1.56 eV/formula unit [50], which provides a measure for the thermodynamic instability of Sn_3N_4. This is in line with the sputter damages occurring upon bombardment with Ar^+ with energies above 200 eV. This metastability will also limit the temperature range, where the material could be used, and possibly also in which environment the materials can be applied. Here the reported stability of γ-Sn_3N_4 (≥300 °C) could be a rough guide for the order of magnitude in question [49].

The sharp decrease in grain size observed upon alloying (Fig. 6) is similar to, but more drastic than, observed in the Al-Ge-N case [23]. A plausible explanation is that different sample bias values were used for the binary and ternary samples: the AlN sample with an average grain size of about 30 nm was deposited with a floating bias, and the ternary samples with grain sizes around or below 10 nm were deposited with a −60 V RF bias. In materials with high enthalpies of formation (ΔG_f) such as transition metal nitrides (TiN, CrN etc.), the used bias voltage of −60 V is too small to cause grain size reduction due to bombardment (assuming ion acceleration in a collision-less sheath). However, for materials with lower enthalpy of formation a reduced sputter damage threshold is expected. This is known for instance for sputter reduction of oxides, where the materials with the lowest ΔG_f show the highest propensity for decomposition and sputter reduction.[83] Similarly, GaN shows surface depletion of N upon exposure to plasma etching in Ar^+ [84]. These examples illustrate that oxides and nitrides of high atomic number metals are prone to sputter damages and sputter reduction. Together with the thermodynamic instability of γ-Sn_3N_4 it seems evident that SnN_x grown under a substrate bias of −60 V develops N deficiency (observed by XPS) as well as sputter damages, leading to a reduced grain size. The distinct decrease in grain size is not directly mirrored in the morphology as seen in the fractured cross sections (Fig. 7), as the transition from a clearly columnar to almost glassy morphology is more gradual.

4.2. Properties and possible applications

The hardness and Young's modulus of the prepared Al-Sn-N coatings described here (17–24 GPa) compares well with that of Al-Ge-N coatings deposited under comparable condition (18–24 GPa). However, the trends with respect to alloying content (Sn or Ge, respectively) are slightly different. For the Al-Ge-N coatings distinct changes, connected to the formation of a secondary phase was observed. As no such microstructural change occurs in the present study, no such breaks are observed. Instead the observed trend can be explained by considering three factors: solid solution hardening (at low Sn content); softening due to increasing number of weak Sn-N bonds (at high Sn content), and variations due to changes in coating texture (dip at 4 at.% Sn), where the (001) texture with the close-packing planes orthogonal to the indentation direction is expected to give a hardening, since the dominating slip-systems in wurtzite structures are in the (001) plane.

As in previous work with Al-Ge-N coatings [23], the absorption edge (and thus the measured optical band gap, E_{04}) shifts with alloying content. In comparison to these results, the range available through tuning is increased with absorption edges up to 510 nm (gap down to 2.4 eV), compared to the ternary Al-Ge-N where a max of 350 nm (minimum of 3.5 eV) was reported. In a similar manner also the range of refractive index is expanded, with a maximum of 2.6 (2.2 for the Al-Ge-N samples). These absorption edges mean that the material can, if placed on a reflective substrate, produce absorption based colours, and thus possibly also be used in decorative coatings. The colour space available for such applications will depend on the band edge (i.e. on coating composition) and thickness; and remains to be mapped out. If the material indeed is single phase, the observed shift of the absorption edge must have its origin in the materials electronic structure and a corresponding change in the band gap edges. Whether this change is caused by the alloying on the metal site, or the possible substoichiometry with respect to nitrogen, cannot be determined from the present data. Theoretical materials simulations could here be of great value, and will thus be prioritised future work.

5. Concluding remarks

The present study has presented the first study of ternary materials in the Al-Sn-N system. Samples have been synthesised in the pseudo binary system AlN-SnN, with up to 24 at.% Sn. Only one phase was observed, an AlN-based solid solution: $(Al_{1-x}Sn_x)N_y$. Coatings appear to be single phase, with x varying between 0 and 0.5, and y close to unity. The attained material is metastable with respect to decomposition into AlN, Sn and N_2, as shown by sputter damage during Ar^+ ion etching. However the material is hard at room temperature, with nanoindentation values of 17–24 GPa, and shows varying colour due to a shifting absorption edge which moves from 211 to 510 nm, corresponding to an optical band gap of 5.9 and 2.4, respectively. Combined with previous studies of AlN-based materials the present study expands the range of

properties (mainly optical) which can be reached by controlled alloying. Possible applications for these materials include optical filters with a tuneable absorption edge, but also decorative coatings, both with the added multifunctionality of also being a hard, and thus presumably a scratch-resistant material. Before the possible application of these materials the stability in different environments must however be determined. Thus possible directions for further studies include stability and application investigations; as well as comparative studies between different Al-A-N systems (A = Si, Ge, Sn); but also a more detailed analysis of the sputter damages for these materials and how to avoid them, as well as *ab-initio* materials simulations in order to understand how alloying effects the electronic structure of the material, and thereby understand the observed changes in optical properties as a function of alloying content.

Acknowledgements

The authors wish to acknowledge the financial support of the Swedish Research Council (VR, ref. no. 623-2010-604 and 623-2013-69), and “Stiftelsen Bengt Lundqvist Minne”; and wish to thank Dr. Max Döbeli at ETH Zürich, for performing ion beam analysis; and Dr. Alex Montagne at Empa Thun, for assistance with nanoindentation.

References

[1] W.-D. Munz, Titanium aluminum nitride films: a new alternative to TiN coatings, J. Vac. Sci. Technol. A Vac. Surfaces, Films 4 (1986) 2717–2725.
[2] O. Knotek, M. Bohmer, T. Leyendecker, On structure and properties of sputtered Ti and Al based hard compound films, J. Vac. Sci. Technol. A Vac. Surfaces, Films 4 (1986) 2695–2700.
[3] S. Veprek, The search for novel, superhard materials, J. Vac. Sci. Technol. A Vac. Surfaces, Films 17 (1999) 2401–2420.
[4] T. Zehnder, J. Matthey, P. Schwaller, A. Klein, P.-A. Steinmann, J. Patscheider, Wear protective coatings consisting of TiC-SiC-a-C: H deposited by magnetron sputtering, Surf. Coatings Technol. 163 –164 (2003) 238–244.
[5] A. Cavaleiro, B. Trindade, M.T. Vieira, The influence of the addition of a third element on the structure and mechanical properties of transition-metal-based nanostructured hard films: part I – nitrides, in: A. Cavaleiro, J.T.M. De Hosson (Eds.), Nanostructured Coatings, Springer Science+Business Media, New York, 2006, pp. 261–314.
[6] B. Trindade, A. Cavaleiro, M.T. Vieira, The influence of the addition of a third element on the structure and mechanical properties of transition-metal-based nanostructured hard films: part II – carbides, in: A. Cavaleiro, J.T.M. De Hosson (Eds.), Nanostructured Coatings, Springer Science+Business Media, New York, 2006, pp. 315–346.
[7] P.H. Mayrhofer, C. Mitterer, L. Hultman, H. Clemens, Microstructural design of hard coatings, Prog. Mater. Sci. 51 (2006) 1032–1114.
[8] O. Wilhelmsson, M. Rasander, M. Carlsson, E. Lewin, B. Sanyal, U. Wiklund, O. Eriksson, U. Jansson, Design of nanocomposite low-friction coatings, Adv. Funct. Mater. 17 (2007) 1611–1616.
[9] J. Houska, J.E. Klemberg-Sapieha, L. Martinu, Atomistic simulations of the characteristics of TiSiN nanocomposites of various compositions, Surf. Coatings Technol. 203 (2009) 3348–3355.
[10] J.E. Krzanowski, S.H. Koutzaki, Mechanical properties of sputter-deposited titanium-silicon-carbon films, J. Am. Ceram. Soc. 84 (2001) 672–674.
[11] C.S. Sandu, R. Sanjinés, M. Benkahoul, F. Medjani, F. Lévy, Formation of composite ternary nitride thin films by magnetron sputtering co-deposition, Surf. Coatings Technol. 201 (2006) 4083–4089.
[12] C.S. Sandu, R. Sanjinés, M. Benkahoul, M. Parlinska-Wojtan, A. Karimi, F. Lévy, Influence of Ge addition on the morphology and properties of TiN thin films deposited by magnetron sputtering, Thin Solid Films 496 (2006) 336–341.
[13] L. Liljeholm, M. Junaid, T. Kubart, J. Birch, L. Hultman, I. Katardjiev, Synthesis and characterization of (0001)-textured wurtzite Al1-xBxN thin films, Surf. Coatings Technol. 206 (2011) 1033–1036.
[14] J.-H. Song, S.-C. Wang, J.C. Sung, J.-L. Huang, D.-F. Lii, Characterization of reactively sputtered c-axis orientation (Al, B)N films on diamond, Thin Solid Films 517 (2009) 4753–4757.
[15] M. Witthaut, R. Cremer, K. Reichert, D. Neuschütz, Characterization of ternary Al–B–N films, Thin Solid Films 377–378 (2000) 478–483.
[16] A. Mazel, P. Marti, F. Henry, B. Armas, R. Bonnet, M. Loubradou, Nanostructure and local chemical composition of AlNSi3N4 layers grown by LPCVD, Thin Solid Films 304 (1997) 256–266.
[17] A. Pélisson, M. Parlinska-Wojtan, H.J. Hug, J. Patscheider, Microstructure and mechanical properties of AleSieN transparent hard coatings deposited by magnetron sputtering, Surf. Coat. Technol. 202 (2007) 884–889.
[18] A. Pélisson, AleSieN Transparent Hard Nanostructured Coatings, Doctoral thesis, University of Basel, Basel, 2009, p. 234.
[19] H. Liu, W. Tang, D. Hui, L. Hei, F. Lu, Characterization of (Al, Si)N films deposited by balanced magnetron sputtering, Thin Solid Films 517 (2009) 5988–5993.
[20] A. Pélisson-Schecker, H.J. Hug, J. Patscheider, Complex phase compositions in nanostructured coatings as evidenced by photoelectron spectroscopy: the case of Al-Si-N hard coatings, J. Appl. Phys. 108 (2010) 023508.
[21] C.A. Pignedoli, D. Passerone, H.J. Hug, A. Pélisson-Schecker, J. Patscheider, Role of negatively charged defects in the lattice contraction of AleSieN, Appl. Phys. Lett. 96 (2010) 071908.
[22] E. Lewin, D. Loch, A. Montagne, A.P. Ehiasarian, J. Patscheider, Comparison of Al-Si-N nanocomposite coatings deposited by HIPIMS and DC magnetron sputtering, Surf. Coat. Technol. 232 (2013) 680–689.
[23] E. Lewin, M. Parlinska-Wojtan, J. Patscheider, Nanocomposite AleGeeN thin films and their mechanical and optical properties, J. Mater. Chem. 22 (2012) 16761–16773.
[24] C.-L. Chang, C.-S. Huang, Effect of bias voltage on microstructure, mechanical and wear properties of AleSieN coatings deposited by cathodic arc evaporation, Thin Solid Films 519 (2011) 4923–4927.
[25] J. Musil, M. Šašek, P. Zeman, R. Čerstvý, D. Heřman, J.G. Han, V. Šatava, Properties of magnetron sputtered AleSieN thin films with a low and high Si content, Surf. Coatings Technol. 202 (2008) 3485–3493.
[26] A. Pélisson-Schecker, H.J. Hug, J. Patscheider, Morphology, microstructure evolution and optical properties of AleSieN nanocomposite coatings, Surf. Coatings Technol. 257 (2014) 114–120.
[27] D. Martínez-Martínez, C. López-Cartes, A. Fernández, J.C. Sánchez-López, Influence of the microstructure on the mechanical and tribological behavior of TiC/a-C nanocomposite coatings, Thin Solid Films 517 (2009) 1662–1671.
[28] T. Zehnder, P. Schwaller, F. Munnik, S. Mikhailov, J. Patscheider, Nanostructural and mechanical properties of nanocomposite nc-TiC/a-C: H films deposited by reactive unbalanced magnetron sputtering, J. Appl. Phys. 95 (2004) 4327–4334.
[29] T. Zehnder, J. Patscheider, Nanocomposite TiC/a-C: H hard coatings deposited by reactive PVD, Surf. Coatings Technol. 133–134 (2000) 138–144.
[30] J. Patscheider, Nanocomposite hard coatings for wear protection, MRS Bull. 28 (2003) 180–183.
[31] H. Wriedt, The AleN (Aluminum-Nitrogen) system,, J. Phase Equilibria 7 (1986) 329–333.
[32] A. McAlister, D. Kahan, The AleSn (Aluminum-Tin) system,, J. Phase Equilibria 4 (1983) 410–414.
[33] M.A. Pietzka, J.C. Schuster, Phase equilibria of the quaternary system Ti Al·Sn·N at 900 °C, J. Alloys Compd. 247 (1997) 198–201.
[34] P. Rogl, J.C. Schuster, SneBeN (Tin-Boron-Nitrogen), in: phase diagrams ternary boron nitride silicon nitride systems, ASM Int. (1992) 94–95.
[35] F. Weitzer, K. Remschnig, J.C. Schuster, P. Rogl, Phase equilibria and structural chemistry in the ternary systems MeSieN and MeBeN (M = Al, Cu, Zn, Ag, Cd, In, Sn, Sb, Au, Tl, Pb, Bi), J. Mater. Res. 5 (1990) 2152–2159.
[36] H.O. Pierson, Handbook of Refractory Carbides and Nitrides, William Andrew Publishing, Westwood, NJ, 1996.
[37] J.A. Kohn, P.G. Cotter, R.A. Potter, Synthesis of aluminum nitride monocrystals, Am. Mineralogist 41 (1956) 355–359.
[38] G.A. Cox, D.O. Cummins, K. Kawabe, R.H. Tredgold, On the preparation, optical properties and electrical behaviour of aluminium nitride, J. Phys. Chem. Solids 28 (1967) 543–548.
[39] A. Brudnik, A. Czapla, E. Kusior, AlN thin films prepared by optical emission spectroscopy-controlled reactive sputtering, Thin Solid Films 478 (2005) 67–71.
[40] V. Mortet, M. Nesladek, K. Haenen, A. Morel, M. D'Olieslaeger, M. Vanecek, Physical properties of polycrystalline aluminium nitride films deposited by magnetron sputtering, Diam. Relat. Mater. 13 (2004) 1120–1124.
[41] J. Bjurstrom, G. Wingqvist, I. Katardjiev, Synthesis of textured thin piezoelectric AlN films with a nonzero C-axis mean tilt for the fabrication of shear mode resonators, ultrasonics, ferroelectrics and frequency control, IEEE Trans. 53 (2006) 2095–2100.
[42] M. Ishihara, S.J. Li, H. Yumoto, K. Akashi, Y. Ide, Control of preferential orientation of AlN films prepared by the reactive sputtering method, Thin Solid Films 316 (1998) 152–157.
[43] V. Brien, P. Pigeat, Microstructures diagram of magnetron sputtered AlN deposits: amorphous and nanostructured films, J. Cryst. Growth 299 (2007) 189–194.
[44] G.F. Iriarte, F. Engelmark, M. Ottosson, I.V. Katardjiev, Influence of deposition parameters on the stress of magnetron sputter-deposited AlN thin films on Si(100) substrates, J. Mater. Res. 18 (2003) 423–432.
[45] G.F. Iriarte, F. Engelmark, I.V. Katardjiev, Reactive sputter deposition of highly oriented AlN films at room temperature, J. Mater. Res. 17 (2002) 1469–1475.
[46] R. Deng, P. Muralt, D. Gall, Biaxial texture development in aluminum nitride layers during off-axis sputter deposition, J. Vac. Sci. Technol. A 30 (2012) 051501.
[47] F. Martin, P. Muralt, M.-A. Dubois, A. Pezous, Thickness dependence of the properties of highly c-axis textured AlN thin films, J. Vac. Sci. Technol. A 22 (2004) 361.
[48] R.S. Lima, P.H. Dionisio, W.H. Schreiner, C. Achete, Magnetron sputtered tin nitride, in: Solid State Communications, 1991, pp. 395–398.

[49] N. Scotti, W. Kockelmann, J. Senker, S. Traßel, H. Jacobs, Sn3N4, ein Zinn(IV)-nitrid – synthese und erste Strukturbestimmung einer binären Zinn–-Stickstoff-Verbindung, Z. für Anorg. Allg. Chem. 625 (1999) 1435–1439.
[50] C.M. Caskey, J.A. Seabold, V. Stevanovic, M. Ma, W.A. Smith, D.S. Ginley, N.R. Neale, R.M. Richards, S. Lany, A. Zakutayev, Semiconducting properties of spinel tin nitride and other IV3N4 polymorphs, J. Mater. Chem. C 3 (2015) 1389–1396.
[51] T. Maruyama, T. Morishita, Tin nitride thin films prepared by radio-frequency reactive sputtering, J. Appl. Phys. 77 (1995) 6641–6645.
[52] Y. Inoue, M. Nomiya, O. Takai, Physical properties of reactive sputtered tin-nitride thin films, Vacuum 51 (1998) 673–676.
[53] R.G. Gordon, D.M. Hoffman, U. Riaz, Low-temperature atmospheric pressure chemical vapor deposition of polycrystalline tin nitride thin films, Chem. Mater. 4 (1992) 68–71.
[54] R.S. Lima, P.H. Dionísio, J.T. Moro, W.H. Schreiner, C. Achete, Thermal evolution and stability of a tin nitride obtained by reactive sputtering, Hyperfine Interact. 83 (1994) 315–319.
[55] L. Maya, Preparation of tin nitride via an amide-imide intermediate, Inorg. Chem. 31 (1992) 1958–1960.
[56] L. Maya, Deposition of crystalline binary nitride films of tin, copper, and nickel by reactive sputtering, J. Vac. Sci. Technol. A Vac. Surfaces, Films 11 (1993) 604–608.
[57] T. Maruyama, Y. Osaki, Effect of electrochemical polarization on optical properties of sputter-prepared tin nitride in aqueous electrolyte, J. Electrochem. Soc. 143 (1996) 326–329.
[58] F. Fischer, G. Ilicvici, Über die Produkte der Lichtbogen- und Funkentladung in flüssigem Argon bezw. Stickstoff. Dritte Mitteilung: Über Zinnstickstoff und pyrophores Zinn, Berichte Dtsch. Chem. Ges. 42 (1909) 527–537.
[59] C.J. Overbeck, Color in films of sputtered tin, J. Opt. Soc. Am. 23 (1933) 109–113.
[60] R. Kamei, T. Migita, T. Tanaka, K. Kawabata, Effect of d.c. bias on the deposition rate using r.f.–d.c. coupled magnetron sputtering for SnNx thin films, Vacuum 59 (2000) 764–770.
[61] D.M. Hoffman, S.P. Rangarajan, S.D. Athavale, D.J. Economou, J.-R. Liu, Z. Zheng, W.-K. Chu, Plasma-enhanced chemical vapor deposition of silicon, germanium, and tin nitride thin films from metalorganic precursors, J. Vac. Sci. Technol. A 13 (1995) 820–825.
[62] J.J. Hantzpergue, J.C. Remy, Propriétés des films étain-azote amorphes réalisés par pulvérisation cathodique réactive-nature de la liaison métal-azote, Thin Solid Films 30 (1975) 205–214.
[63] T. Lindgren, M. Larsson, S.-E. Lindquist, Photoelectrochemical characterisation of indium nitride and tin nitride in aqueous solution, Sol. Energy Mater. Sol. Cells 73 (2002) 377–389.
[64] W. Janeff, Herstellung von Metallnitriden in der Glimmentladung und einige ihrer Eigenschaften, Zeitschrift für Physik A Hadrons Nucl. 142 (1955) 619–636.
[65] D. Lützenkirchen-Hecht, R. Frahm, Structure of reactively sputter deposited tin-nitride thin films: a combined X-ray photoelectron spectroscopy, in situ X-ray reflectivity and X-ray absorption spectroscopy study, Thin Solid Films 493 (2005) 67–76.
[66] N. Takahashi, T. Nakamura, Tin nitride thin films with room-temperature visible emission, Electrochem. Solid-State Lett. 8 (2005) C63–C64.
[67] P.E. Larson, M.A. Kelly, Surface charge neutralization of insulating samples in x-ray photoemission spectroscopy, J. Vac. Sci. Technol. A 16 (1998) 3483–3489.
[68] W.K. Chu, J.W. Mayer, M.A. Nicolet, Backscattering Spectrometry, Academic Press, 1978.
[69] C. Kottler, M. Döbeli, F. Glaus, M. Suter, A spectrometer for low energy heavy ion ERDA, Nucl. Instrum. Methods Phys. Res. Sect. B Beam Interact. Mater. Atoms 248 (2006) 155–162.
[70] L.R. Doolittle, A semiautomatic algorithm for rutherford backscattering analysis, Nucl. Instrum. Methods Phys. Res. Sect. B Beam Interact. Mater. Atoms 15 (1986) 227–231.
[71] C. Jeynes, et al., Elemental thin film depth profiles by ion beam analysis using simulated annealing – a new tool, J. Phys. D Appl. Phys. 36 (2003) R97.
[72] W.C. Oliver, G.M. Pharr, An improved technique for determining hardness and elastic modulus using load and displacement sensing indentation experiments, J. Mater. Res. 7 (1992) 1564–1583.
[73] G.G. Stoney, The tension of metallic films deposited by electrolysis, in: Proceedings of the Royal Society of London. Series A, 82, 1909, pp. 172–175.
[74] C.A. Klein, How accurate are Stoney's equation and recent modifications, J. Appl. Phys. 88 (2000) 5487–5489.
[75] G.C.A.M. Janssen, M.M. Abdalla, F. van Keulen, B.R. Pujada, B. van Venrooy, Celebrating the 100th anniversary of the Stoney equation for film stress: developments from polycrystalline steel strips to single crystal silicon wafers, Thin Solid Films 517 (2009) 1858–1867.
[76] R. Swanepoel, Determination of the thickness and optical constants of amorphous silicon, J. Phys. E Sci. Instrum. 16 (1983) 1214.
[77] S. Dirk Poelman, Philippe Frederic, Methods for the determination of the optical constants of thin films from single transmission measurements: a critical review, J. Phys. D Appl. Phys. 36 (2003) 1850.
[78] I. Bertóti, Characterization of nitride coatings by XPS, Surf. Coatings Technol. 151–152 (2002) 194–203.
[79] A. Pélisson-Schecker, H.J. Hug, J. Patscheider, Charge referencing issues in XPS of insulators as evidenced in the case of AleSieN thin films, Surf. Interface Analysis 44 (2012) 29–36.
[80] H.F. McMurdie, M.C. Morris, E.H. Evans, B. Paretzkin, J.H. de Groot, C.R. Hubbard, S.J. Carmel, Standard X-ray diffraction powder patterns, Natl. Bur. Stand. (US) Monogr. 25 (section 12) (1975) 5.
[81] G.B. Harris, Quantitative measurement of preferred orientation in rolled uranium bars, Philos. Mag. Ser. 7 (43) (1952) 113–123.
[82] P. Scardi, M. Leoni, R. Delhez, Line broadening analysis using integral breadth methods: a critical review, J. Appl. Crystallogr. 37 (2004) 381–390.
[83] A.B. Christie, J. Lee, I. Sutherland, J.M. Walls, An XPS study of ion-induced compositional changes with group II and group IV compounds, Appl. Surf. Sci. 15 (1983) 224–237.
[84] C.R. Eddy Jr., B. Molnar, Plasma etch-induced conduction changes in gallium nitride, J. Elec Materi 28 (1999) 314–318.